BIOCHEMISTRY
including biophysical chemistry & molecular biology
Article

Biochemistry **2010,** *49,* 8143–8154 8143
DOI: 10.1021/bi1006354

Interaction Kinetic and Structural Dynamic Analysis of Ligand Binding to Acetylcholine-Binding Protein†

Matthis Geitmann,‡ Kim Retra,§ Gerdien E. de Kloe,∥ Evert Homan,‡ August B. Smit,⊥ Iwan J. P. de Esch,∥ and U. Helena Danielson*,‡,#

‡*Beactica AB, Box 567, SE-751 22 Uppsala, Sweden,* §*Leiden/Amsterdam Center for Drug Research (LACDR), Division of BioMolecular Analysis, Department of Chemistry and Pharmaceutical Sciences, Faculty of Sciences, VU University, Amsterdam, The Netherlands,* ∥*Leiden/Amsterdam Center for Drug Research (LACDR), Division of Medicinal Chemistry, Department of Chemistry and Pharmaceutical Sciences, Faculty of Sciences, VU University, Amsterdam, The Netherlands,* ⊥*Department of Molecular and Cellular Neurobiology, Center for Neurogenomics and Cognitive Research, Neuroscience Campus Amsterdam, VU University, Amsterdam, The Netherlands, and* #*Department of Biochemistry and Organic Chemistry, Uppsala University, BMC, Box 576, SE-751 23 Uppsala, Sweden*

Received April 25, 2010; Revised Manuscript Received July 28, 2010

ABSTRACT: The mechanism of agonist interactions with Cys-loop ligand-gated ion channels has been studied using the acetylcholine-binding protein (AChBP) from *Lymnaea stagnalis* as a model protein and acetylcholine, nicotine, epibatidine, and a series of substituted quinuclidines as ligands. A biosensor-based assay for direct interaction studies of immobilized AChBP and small molecule ligands was developed. It allowed the characterization of the interaction kinetics of the ligands and the structural dynamics of the protein. The interactions with AChBP were very sensitive to variations in the experimental conditions and showed several types of complexities. These could be resolved into two types of ligand-induced secondary effects with different kinetics, representing fast and slow conformational changes. The data could be rationalized in a mechanistic model, and a structural interpretation of the interaction was obtained by molecular modeling involving induced fit and loop flexibility simulations. The data suggest that AChBP exhibits ligand-induced structural dynamics, as expected for the ligand gating mechanism of Cys-loop receptors. It shows that the formation of the initial encounter complex between AChBP and ligands is very rapid, in accordance with the functional characteristics required of neurotransmission. These developed procedures will enable further exploration of the mechanism of Cys-loop receptor function and the identification of specific ligands suitable for pharmacological use.

The activation of ligand-gated ion channels by released neurotransmitters is a critical step in neural signaling. Cys-loop receptors constitute an important class of ion channels involved in this process. It includes the nicotinic acetylcholine[1] (nAChR), γ-aminobutyric acid (GABA), serotonin (5-HT_3), and glycine receptors (*1*, *2*). Although major advances in the functional understanding of these receptors have been made in recent years, the mechanism by which agonists and antagonists activate or modulate the function of these receptors is still under investigation (*3*). Also, the structural features required of ligands acting as agonists or antagonists have remained elusive (*4*). This is severely hampering structure-based drug design approaches to target Cys-loop receptors for pharmaceutical purposes (*5*). The present study has been performed in order to obtain a better understanding of the mechanism of the interactions between agonists and Cys-loop receptors.

The soluble acetylcholine-binding protein (AChBP) from the freshwater mollusk *Lymnaea stagnalis* (Ls) (*6*, *7*) was used as a model system so as to avoid the complexities of the membrane spanning domains of the ion channel. It is a well-established structural and functional surrogate for the extracellular domain of Cys-loop receptors and was reasoned to be a suitable model system also for these studies. Ls-AChBP shares a 26% sequence identity with the extracellular receptor domain of the human α7 nicotinic acetylcholine receptor (nAChR) subtype and has similar pharmacological properties (*2*, *6*). X-ray crystal structures of AChBP (*7*−*10*) have contributed much to the understanding of the structural organization, molecular dynamics, and ligand recognition of ligand-gated ion channels. These studies have also demonstrated that AChBP pentamers have a binding site for agonists and antagonists located at the interface between two subunits, equivalent to that for the Cys-loop receptor ion channels. It is composed of a pocket of aromatic and hydrophobic resides from both subunits (*9*). Although agonists and antagonists bind to the same pocket, they stabilize the receptor in different conformational states, thereby giving rise to different functional effects. In contrast to many homologous channels (*11*), the AChBPs show no cooperativity between the multiple binding sites (*6*, *8*, *10*), and the interaction can principally be described by the classical Monod−Wyman−Changeux model (*12*). Furthermore, even if agonists bind with higher affinity to the open state receptor conformation, there is no direct coupling between channel conductance state and receptor occupancy; the channel has been found to be able to open and close several times during a

†This work was supported by a grant from the Seventh Framework Programme of the Commission of the European Communities (HEALTH-F4-2008-202088). G.E.d.K. was supported by the Dutch Top Institute Pharma (project number D2.103: New Approaches for Ligand-Gated Ion Channel Drug Discovery).

*To whom correspondence should be addressed. Tel: +46 18 4714545. Fax: +46 18 558431. E-mail: helena.danielson@beactica.com.

[1]Abbreviations: AChBP, acetylcholine-binding protein; ECD, extracellular domain; GABA, γ-aminobutyric acid; 5-HT, serotonin; IFD, induced fit docking; Ls, *Lymnaea stagnalis*; nAChR, nicotinic acetylcholine receptor; RU, response unit; SPR, surface plasmon resonance.

Published on Web 08/12/2010

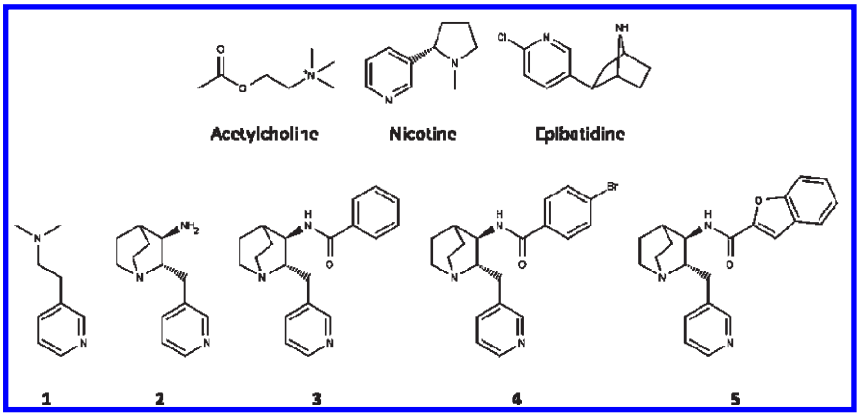

FIGURE 1: Structures of the Cys-loop receptor agonists used in this study.

single agonist receptor occupancy (*13*, *14*). In Cys-loop receptors, ligand-induced conformational changes in the extracellular domain (ECD) involve the characteristic Cys loop as well as other loops, which trigger the opening of the channel. There are several steps involved, each defined by microscopic rate constants, that contribute to the overall efficacy of a ligand (*14*).

In order to access the details of the interaction mechanism and kinetics of nAChR ligands, we developed a surface plasmon resonance (SPR) biosensor-based assay for AChBP. We have previously exploited this technology for kinetic and mechanistic studies of many different protein−ligand systems, a number of which also involved conformational changes and multiple states (*15*−*18*). This time-resolved direct binding method can also be used for the identification of ligands that are suitable for pharmacological use. We have therefore used biosensor-based approach also for screening of ligands against AChBP, both in a direct and an indirect mode (*19*), and for studies of interactions with α-conotoxins, using streptavidin capture of biotinylated AChBP (*20*). During the course of this project, an indirect method for analysis of α-bungarotoxin interactions with AChBP, involving the immobilization of α-bungarotoxin, has also been designed independently by another group (*21*). Although indirect assays have several advantages, they are not applicable for the direct screening or characterization of multiple agonists. In contrast, the current method is well suited for such studies. It has, for example, recently been exploited also for analysis of a series of fragments of known nAChR agonists, validating the approach by comparison with a radioligand assay (de Kloe et al., manuscript submitted). For the present study, the assay and data analysis was optimized so that the mechanistic complexities of agonist interactions with AChBP could be resolved. In addition, this experimental technique was complemented by molecular modeling simulations, allowing structural interpretation of the data. Since the ligand-binding site of AChBP is highly adaptable to different ligands (*8*, *10*, *22*), an induced fit docking protocol that also allows for full flexibility in selected loop regions (*23*) was employed.

The ligands of interest (Figure 1) were previously identified Cys-loop receptor agonists. They included the endogenous neurotransmitter acetylcholine and the natural alkaloids nicotine and epibatidine, occurring in plants in the Solanaceae family and the skin of a poisonous frog, respectively. In addition, a series of quinuclidine derivatives were studied. They are highly selective ligands for the α7 nAChR subtype, which is structurally analogous to the AChBP. The adopted methodology and this set of ligands revealed unexpected complexities in the interactions in the binding between AChBP and small molecule agonists, indicating the involvement of secondary processes. These can be structurally and mechanistically interpreted in the contextual framework of Cys-loop receptor function.

MATERIALS AND METHODS

Compounds. Acetylcholine, nicotine, and epibatidine were purchased from Sigma (St. Louis, MO). The quinuclidine analogues **1** and **2** (Figure 1) were synthesized as described in de Kloe et al. (manuscript submitted) while analogues **3**, **4**, and **5** (Figure 1) were synthesized according to previously published procedures (*24*).

Protein. The acetylcholine-binding protein from *L. stagnalis* (Swiss-Prot P58154) was expressed using the Bac-to-Bac baculovirus expression system (Invitrogen, Carlsbad, CA) following the manufacturer's recommendations. Secreted protein was trapped on a HIS-Select cartridge (Sigma, St. Louis, MO). The cartridge was washed with 24 mL of 10 mM imidazole, left overnight at 4 °C in 250 mM imidazole, and thereafter eluted with 5 mL of 250 mM imidazole. The concentration of imidazole was significantly reduced by using a Slide-A-Lyzer dialysis cassette (Pierce, Rockford, IL) according to the manufacturer's recommendations. The purity of the protein was checked on an SDS gel, and the protein concentration was determined by Bradford analysis. Protein aliquots were stored at −80 °C until use.

Sensor Surface Preparation. The biosensor experiments were performed using Biacore T100 and S51 instruments (GE Healthcare, Uppsala, Sweden). Flow cells on a CM5 chip (GE Healthcare) were activated by using a 1:1 mixture of 0.1 M: 50 mM *N*-hydroxysuccinimide and 200 mM *N*-ethyl-*N*′-((dimethylamino)propyl)carbodiimide for 10 min. AChBP was diluted to 0.04 mg/mL into 50 mM sodium acetate, pH 5.5, and injected over the surface to produce densities between 3 and 20 kRU. For some experiments, AChBP was cross-linked (*25*) with a 7 min injection of the activation mixture after coupling to the surface. The surfaces were subsequently blocked with ethanolamine (1 M, pH 8.5).

Interaction Experiments. Interaction experiments were performed at 25 °C using a running buffer composed of 10 mM sodium phosphate, pH 7.4, 137 mM NaCl, 3 mM KCl, and 0.05% Tween, at a flow rate of 90 mL/min. For some experiments 5% DMSO was added to the running buffer with adjustment to pH 7.4. Compounds were diluted in the running buffer and injected for 60 s at increasing concentrations over the immobilized AChBP. Standard multicycle kinetic analysis (i.e., repeated injections over the same surface with a regeneration step between subsequent injections) was performed for all compounds but

epibatidine in buffer without DMSO. The slow dissociation kinetics of epibatidine in the absence of DMSO were best analyzed by single-cycle kinetic analysis, using essentially the procedure described by Karlsson et al. (*26*).

Data Analysis. Data were double referenced by subtracting signals from (1) an untreated reference channel and (2) responses from blank injections, from the raw signals of sample injections. To determine kinetic parameters, a simple 1:1 interaction model, including a term for limited mass transport, was globally fitted to association and dissociation phase data, using the T100 evaluation software (GE Healthcare). The presented standard deviations are based on at least four replicate series. Simulation of sensorgrams was performed using the BIAevaluation software 3.02 (GE Healthcare).

Molecular Modeling. All molecular modeling studies were performed with Schrödinger Suite 2009, Update 1 (Schrödinger Inc., New York), running on a quad-core Linux workstation. The crystal structure of Ls-AChBP in complex with nicotine, 1UW6.pdb (*10*), was prepared using the Protein Preparation Workflow. The C, D, and E chains, nicotine, and all water molecules beyond 5 Å of a Het group were removed. Different ionization and tautomeric states were generated for nicotine, and the state with the lowest energy penalty was selected. H-bond assignments for Asn, Gln, and His residues were optimized automatically, and water orientations were exhaustively sampled. Finally, the corrected structure was minimized in the OPLS2005 force field to relieve strain until an rmsd of 0.30 was reached.

Starting conformations of the ligands were prepared with ligprep. Epik was used to generate different ionization states. Only the species with the lowest state penalty was retained. Consequently, none of the ligands had protonated pyridine nitrogens, and for compound **2** only the quinuclidine nitrogen was protonated. Since compounds **2**−**5** are racemic mixtures of *trans* isomers, both their (2*S*,3*R*)- and (2*R*,3*S*)-enantiomers were considered during docking. Acetylcholine, nicotine, and epibatidine were included for reference purposes.

The Induced Fit Workflow was used to set up the induced fit docking (IFD) simulations (*23*) in conjunction with loop sampling (*27*, *28*) of loop C. The combined process comprises four stages: (1) generation of an ensemble of protein structures by loop sampling; (2) docking of the ligands to the protein structure ensemble with Glide; (3) optimization of residue side chains surrounding the docked ligand poses with Prime; (4) redocking of the ligands to the induced protein structures with Glide, followed by ranking. Stages 2−4 can be configured through the Induced Fit Workflow GUI, while the preceding loop sampling stage can be added by manually editing the input file created for stages 2−4. For the initial Glide docking stage, the centroid of nicotine, as bound between the A and B chains of 1UW6, was used to define the center of the docking grid box. The box size was set to 20 Å. Up to 10 poses were generated for each ligand with Glide SP (*29*, *30*). Van der Waals scaling for both protein and ligand atoms was set to 0.5. For the induced fit step, the side chains of all residues within 5 Å of the Glide SP ligand poses were optimized using Prime. The final redocking step was performed with Glide XP (*31*). Ligands were redocked into structures with energies within 30.0 kcal/mol of the best structure and within the top 10 structures overall. The final poses thus obtained were ranked by the IFD score, calculated as the sum of the Glide XP docking score and 0.05 × the Prime energy of the protein−ligand complex. The resulting input file was written out and manually edited to enable the loop sampling stage by uncommenting the appropriate lines and specifying the loop to be sampled from Val183 to Tyr192 in the A subunit. Only structures with energies within 30.0 kcal/mol of the lowest energy structure and up to a maximum of 5 structures were retained.

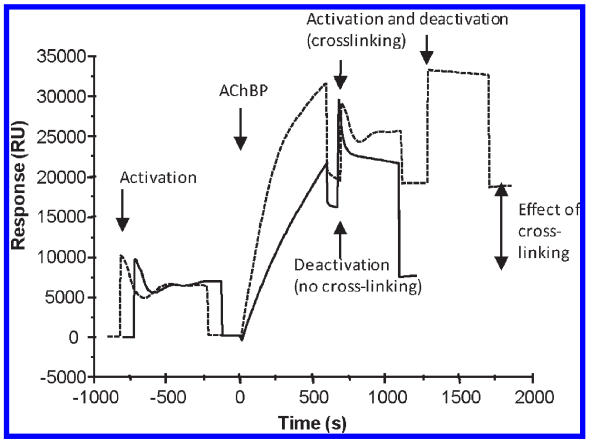

FIGURE 2: Sensorgrams for the immobilization of AChBP by amine coupling with cross-linking (· · ·) and without cross-linking (—).

The molecular volumes of the ligands in their best scoring IFD poses were calculated using QikProp (*32*). Sequence alignments were performed with the Multiple Sequence Viewer implemented in the Schrödinger software. All images were prepared with PyMol 0.99 (*33*).

RESULTS

Sensor Surface Characteristics. The immobilization of AChBP to the sensor matrix by the standard amine coupling protocol resulted in sensor surface densities of AChBP of up to 10 kRU. However, a massive loss of preconcentrated but noncovalently bound AChBP was observed during the deactivation injection with ethanolamine (1 M, pH 8.5). By cross-linking the protein with an injection of NHS/EDC before the ethanolamine injection, the loss of material from the surface was much smaller, and up to 20 kRU could consequently be obtained (Figure 2). Higher immobilization levels increased the signal amplitudes for ligand interactions but since cross-linking interfered with the dynamics of the protein (see below), it was not used routinely. Prepared surfaces were relatively stable and could be used for 100 interaction cycles without loss of more than 20% of the binding capacity. The preparation of a single surface required about 2 μg of protein.

The apparent binding capacity of the AChBP surfaces was up to 50−70%, as judged by the maximal signal levels (R_{max}) for the tested ligands. However, it was not possible to obtain an exact value since the R_{max} values varied for the different ligands (as detailed below under Fast Secondary Effects). Cross-linked surfaces had similar binding capacities as non-cross-linked surfaces but did not exhibit the secondary effects, suggesting that cross-linking interfered with the ligand-induced dynamics of the protein (see Slow Secondary Effects below).

Interaction Analysis. Experiments were initially performed with acetylcholine, nicotine, and epibatidine (Figure 1), three structurally diverse small molecule agonists with very different interaction characteristics for AChBP. A series of quinuclidines with varying size (Figure 1) was subsequently studied in order to explore some of the discovered mechanistic complexities in the interactions.

The interactions of agonists with AChBP was measured by serial 1 min injections of increasing concentrations of each

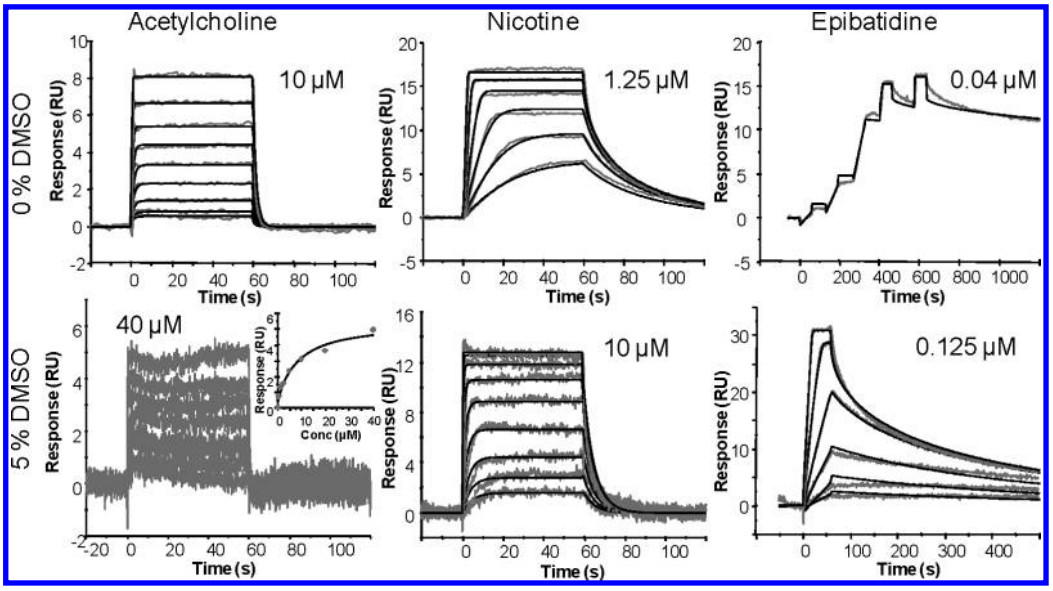

FIGURE 3: Sensorgrams for the interaction between immobilized AChBP and agonists (acetylcholine, nicotine, epibatidine) with or without 5% DMSO in the buffer. The sensorgrams represent 2-fold (acetylcholine and nicotine) or 4-fold dilution series (epibatidine) from the highest concentration (specified in each graph). Theoretical curves (black), obtained by global nonlinear regression analysis using a 1:1 interaction model with a term for mass transport, are overlaid on the experimental traces from multicycle experiments (gray). The analysis of slow dissociating epibatidine in the absence of DMSO was based on single cycle experiments (*26*).

Table 1: Affinities and Apparent Rate Constants for the Interaction between AChBP and Agonists (Acetylcholine, Nicotine, Epibatidine, and a Series of Quinuclidine Derivatives, **1-5**) in the Presence and Absence of 5% DMSO in the Buffer

		k_{on} (10^6 M^{-1} s^{-1})	k_{off} (s^{-1})	K_D (nM)
0% DMSO	acetylcholine	(0.956 ± 0.217)[a]	(0.432 ±0.061)[a]	458 ± 39
	nicotine	> 10	nd[b]	40.7 ± 9.9
	epibatidine	> 10	nd	0.0835 ± 0.0303
5% DMSO	acetylcholine	nd	> 1	3850 ± 980
	nicotine	12.5 ± 6.21	3.62 ± 1.48	310 ± 61
	epibatidine	> 10	nd	2.67 ± 1.34
	1	nd	nd	4250 ± 910
	2	nd	nd	345 ± 40
	3	nd	nd	141 ± 47
	4	nd	nd	53.5 ± 45
	5	nd	nd	12.8 ± 4.3

[a]Apparent rate constants, determined under the assumption that the interaction was not influenced by limited mass transport. [b]nd: not possible to determine due to fast kinetics.

compound until a steady-state maximum binding level was approached (association phase). The subsequent dissociation of the agonist (dissociation phase) was also monitored (Figure 3). The recorded sensorgrams were subjected to global nonlinear regression analysis, using a 1:1 interaction model where the on- and off-rates (Table 1) were extracted simultaneously from the association and the dissociation phases. The ligands all interacted with very rapid kinetics, limiting the possibility of quantifying the rate constants. A term accounting for limited mass transport was therefore included in the model (*34*), identifying the interactions which were outside of the analytical window of this technique, as specified under Kinetic Analysis (see below). Curiously, there were initially some qualitative and quantitative variations between sensorgrams obtained in different experiments, indicating that the interactions were very sensitive to the handling of the protein before immobilization and/or the experimental conditions for the interaction measurements. One parameter that was found to have an exceptionally large impact on the interactions was the concentration of DMSO in the assay. Experiments were therefore carried out in buffer without DMSO, as well as in buffer containing 5% DMSO (Figure 3). In addition, in some experiments, significant secondary effects gave rise to sensorgrams that clearly differed from a simple 1:1 model (see below). These were excluded from the quantitative analysis, and parameter values were consequently only determined using sensorgrams that were well described by a 1:1 interaction model (Figure 3 and Table 1).

Since steady-state binding levels were not influenced by mass transport effects, the analysis allowed the estimation of affinities for all compounds, despite the rapid kinetics. The affinities and the binding capacity of the protein were clearly lower in the presence of 5% DMSO. This partially reversible reduction in binding capacity appeared to be different for the three ligands, typically 20−40% for epibatidine and nicotine and 40−70% for acetylcholine, accounting for the higher noise in the sensorgrams recorded in the presence of DMSO (Figure 3). The effect of DMSO on the individual rate constants could not be determined since these were outside the range that can be measured in at least one of the tested buffer conditions (see below).

Kinetic Analysis. The rapid kinetics of the interactions required careful analysis of the data to ensure that the parameter

estimates were reliable. This was judged by the congruity of the rate constants obtained from the analysis of at least four measurement series. Accordingly, rate constants could only be determined for nicotine and when the buffer contained DMSO, i.e., when the affinity was reduced by the presence of solvent.

The mass transport term in the regression analysis of the sensorgrams for acetylcholine did not indicate that the interactions were mass transport limited in the absence of DMSO, and congruent association rates and dissociation rates were obtained from the analysis. However, simulation of sensorgrams demonstrated that also the interaction with acetylcholine was influenced by limited mass transport (Figure 4A). In the first case, a sensorgram for acetylcholine was simulated using the estimated affinity (K_D = 458 nM, Table 1) and a mass transport constant typically obtained in this study for nicotine ($k_t = 5 \times 10^6$ RU M^{-1} m s^{-1}) and an association rate constant previously determined by stopped flow ($k_{on} = 1.1 \times 10^8$ M^{-1} s^{-1})(*35*). The corresponding value for the dissociation rate constant was consequently obtained as $k_{off} = k_{on}K_D = 50$ s^{-1}. The simulated sensorgram was indistinguishable from the experimental sensorgram (Figure 4A),

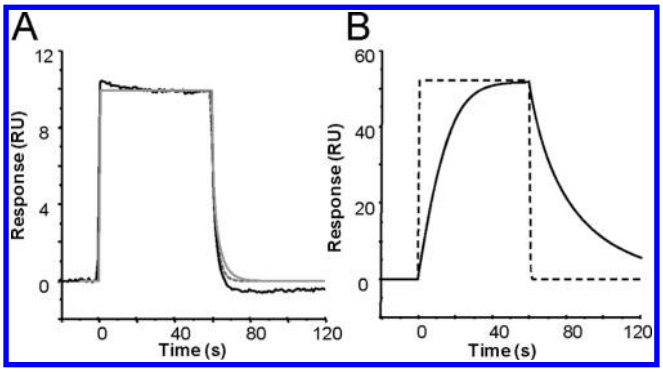

FIGURE 4: Analysis of mass transport limitations in experimental data by comparison with simulated sensorgrams. (A) Sensorgrams of the interaction between acetylcholine (5 μM) and AChBP. Theoretical curves from a global regression analysis (dotted gray) and a simulation of the interaction assuming a 120-fold faster kinetics and a term for limited mass transport (gray) are overlaid on an experimental sensorgram (black) recorded with acetylcholine. (B) Simulated sensorgrams for the interaction between 10 μM nicotine and AChBP using a 1:1 binding model with mass transport (black) and without mass transport (dotted black). The rate constants are based on determined values for nicotine in buffer with 5% DMSO ($k_{on} = 1.25 \times 10^7$ M^{-1} s^{-1}, $k_{off} = 3.62$ s^{-1}), and a mass transport coefficient $k_t = 10^7$ RU M^{-1} m s^{-1}.

showing that association and dissociation rates were above the limit of what can be accurately determined. A second simulation (Figure 4B), based on the association and dissociation rate constants determined for nicotine with and without terms for limited mass transport (Table 1), highlights the effect of limited mass transport. The curvature in the association and dissociation phases of the sensorgram results from the rebinding of the compounds that is faster than the mass transport of the compound from the surface. The interactions were also too fast for accurate estimation of the association and dissociation rate constants for quinuclidine analogues (see Fast Secondary Effects).

Slow Secondary Effects. In many of the experiments, the sensorgrams deviated significantly from a simple 1:1 interaction. A peculiar, but characteristic and recurring, dose-dependent slow signal reduction was often observed during the injection phase (Figure 5). Following reference correction, sensorgrams showed negative signals after 1 min injections of agonist. The signal returned slowly back to baseline level with a rate that was slower than the apparent dissociation of the ligand, best exemplified with nicotine.

The possibility of unspecific binding or other instrument-related artifacts could be excluded after careful inspection of the raw data and the reference surface (see Figure 5 insets). The phenomenon was always observed, irrespective of the instrument used. However, the effect varied for different surface preparations, suggesting that it was sensitive to the conditions for immobilization. It was most pronounced when experiments were performed with surfaces made with fresh AChBP. It was also very sensitive to the buffer conditions and most obvious when measured without DMSO in the buffer. Desensitization of the receptor against this effect was observed when surfaces were exposed to a series of identical injections with short dissociation times (Figure 6A). The surface regained sensitivity with longer waiting time between injections (data not shown). Cross-linking reduced the agonist-induced negative signal change (Figure 6B).

Based on these observations, it was concluded that the slow signal changes were caused by ligand-induced conformational changes. These are accounted for in a mechanistic model containing the different states expected for Cys-loop receptors (Scheme 1). The order of magnitude of the rates describing the equilibrium between the two ligand bound states was estimated for nicotine by simulation of sensorgrams using this mechanistic model. The simulation was based on reported values for nicotine, $k_1 = 1.5 \times 10^8$ s^{-1} M^{-1} and $k_{-1} = 5.7$ s^{-1} (*35*), and the assumption that

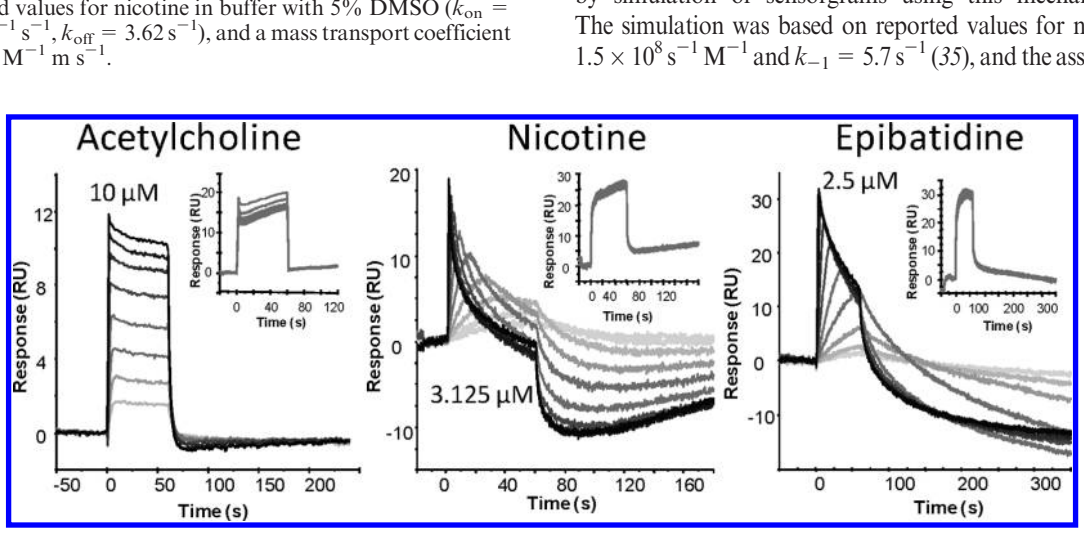

FIGURE 5: Sensorgrams for acetylcholine, nicotine, and epibatidine with strong secondary effects indicating slow agonist-induced conformational changes of AChBP. The sensorgrams represent 2-fold concentration series from the highest concentration (specified in each graph), recorded in the absence of DMSO. Raw data sensorgrams from reference surfaces are shown in the insets.

$k_1 = k_{-3}, k_{-1} = k_3, k_2 = k_{-4}, k_{-2} = k_4$ (Scheme 1), and $k_t = 10^7$ RU M^{-1} m s^{-1}. Similar sensorgrams to the experimental sensorgrams were generated with $k_2 = 0.05\ s^{-1}$ and $k_{-2} = 0.01\ s^{-1}$ (Figure 7), providing rough estimates of the values of these rate constants. The magnitude of the secondary effects was different for acetylcholine, epibatidine, and nicotine (Figure 5), indicating that the structure of the agonist was important for inducing the effect.

Fast Secondary Effects. In addition to the large signals resulting from the slow conformational effects on the shape of sensorgrams, a more subtle effect arising from a form of fast ligand-induced biosensor changes was also observed. It was evident from the large differences in the maximal signal amplitudes for acetylcholine, nicotine, and epibatidine (Figure 3). Despite similar molecular weights, acetylcholine had a 2 times lower R_{max} than nicotine (in the absence of DMSO in the buffer). In the presence of 5% DMSO, the difference in R_{max} was increased to 4 times. This effect contributed to the magnitude of the observed signals but was too fast to be distinguished by its curvature in sensorgrams from the regular binding signal.

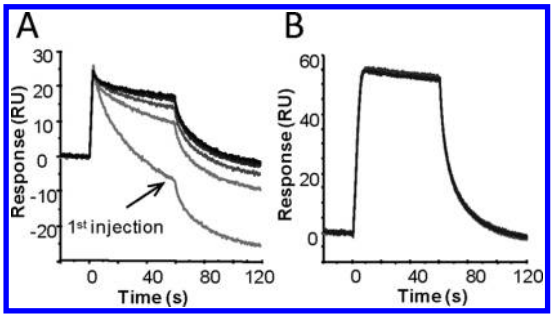

FIGURE 6: Desensitization against slow ligand-induced changes in AChBP. Sensorgrams of repeated injections of 1 μM nicotine over (A) non-cross-linked and (B) cross-linked AChBP, immobilized to parallel surfaces of a CM5 biosensor chip.

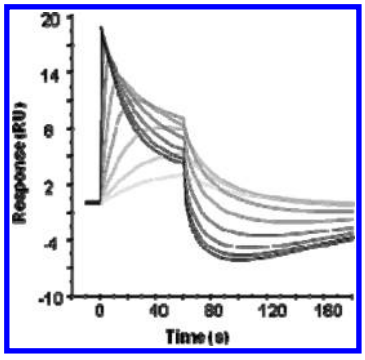

FIGURE 7: Simulated sensorgrams for the interaction between nicotine and AChBP according to Scheme 1. The simulation was based on $k_1 = 1.5 \times 10^8\ s^{-1}\ M^{-1}$, $k_{-1} = 5.7\ s^{-1}$, $k_2 = 0.05\ s^{-1}$, $k_{-2} = 0.01\ s^{-1}$, and $k_t = 10^7$ RU M^{-1} m s^{-1} and the assumption that $k_1 = k_{-3}$, $k_{-1} = k_3$, $k_2 = k_{-4}$, and $k_{-2} = k_4$. The sensorgrams represent 2-fold concentration series of nicotine, with 3.125 μM as the highest concentration.

Scheme 1: Illustration of a "Minimalist Model" of Cys-Loop Receptor Function Involving the Molecular Species (R, Receptor; A, Agonist) and the Different States (*, Activated/Open State; D, Desensitized State) and the Transitions Involved[a]

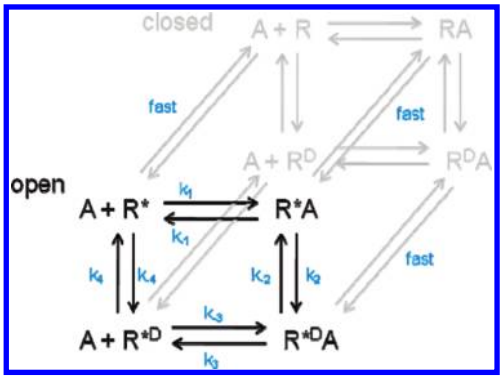

[a]The rate constants used for simulations are specified.

In order to explore the interaction characteristics as a function of the structural features of AChBP ligands, the interactions of a series of quinuclidine analogues were also investigated (Figure 8 and Table 1). The affinities were clearly proportional to the size of the molecule, with the smallest molecule (**1**) exhibiting an affinity similar to acetylcholine. After normalization of the signals for the molecular weights of the ligands and the different binding capacities of the surfaces, the determined R_{max} values for the different quinuclidine derivatives differed by almost 50% (not shown). The R_{max} values, as determined by multicycle analysis in the presence of DMSO in the buffer and normalized with respect to the molecular weight of the compounds, were correlated ($r = 0.86$) with the molecular volumes of quinuclidines, acetylcholine, nicotine, and epibatidine (Figure 9A). Less correlation ($r = 0.54$) was found with the affinity of the compounds, as visualized in Figure 9B.

Molecular Modeling. In order to rationalize the dependence of the induced structural changes on the molecular volumes of the ligands, molecular modeling was used. An IFD protocol that allows for full flexibility in selected loop regions (*23*) was employed to obtain plausible ligand-binding hypotheses of this flexible protein. The method is complementary to a recent study by Babakhani et al. (*36*), who used a relaxed-complex molecular dynamics simulation approach to account for protein flexibility while performing virtual screening. The initial loop sampling stage yielded five low-energy conformations of loop C, the loop that caps the entrance to the agonist-binding site. All five had adopted a closed conformation. Comparisons of these loop conformations with the crystal structure for AChBP in complex with nicotine (1UW6) revealed

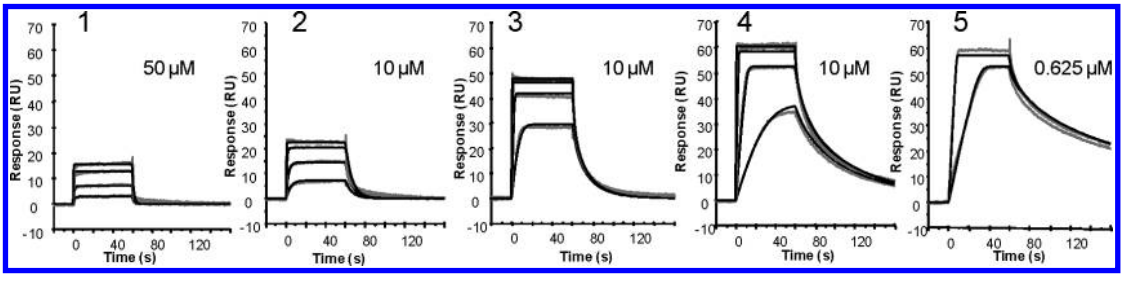

FIGURE 8: Sensorgrams of the interaction between AChBP and quinuclidine-derived analogues **1**−**5**, tested in 4-fold dilution series of the highest concentration given in each graph. Theoretical curves (black) obtained by global nonlinear regression analysis using a 1:1 interaction model with a term for limited mass transport are overlaid on the experimental traces (gray).

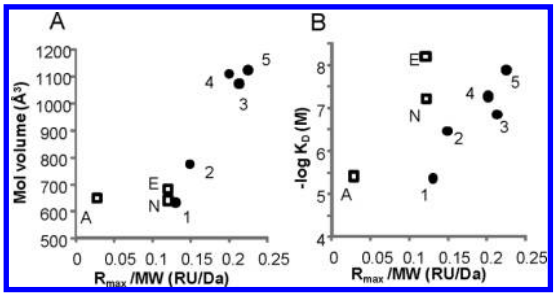

FIGURE 9: Correlation plot between R_{max} values normalized with respect to molecular weight of the compounds and (A) calculated molecular volumes and (B) affinities, determined by multicycle analysis in the presence of DMSO in the buffer for quinuclidine analogues (black dots), acetylcholine (A), nicotine (N), and epibatidine (E) (open squares).

that one of them was very similar to the conformation in the crystal structure (rmsd 1.80 Å for all atoms of residues 183−192).

Subsequent ensemble docking of acetylcholine, nicotine, epibatidine, and compounds **1**−**5** to each of these five AChBP models with different loop C conformations, followed by side-chain optimization, redocking, and scoring yielded the final optimized docking poses for the ligands under investigation. Superpositions of the best scoring IFD solutions of all ligands are shown in Figure 10.

Since compounds **2**−**5** comprise racemic mixtures of *trans* isomers, modeling was performed both for the (2*S*,3*R*)- and the (2*R*,3*S*)-enantiomers. The (2*S*,3*R*)-enantiomers of **2**−**5** showed more consistent binding modes and H-bonding patterns than their (2*R*,3*S*)-enantiomers, although the IFD scores for (2*S*,3*R*)-**2**, **3**, and **5** were marginally higher than for the corresponding (2*R*,3*S*)-enantiomers (1.33, 1.02, and 1.47 kcal/mol, respectively). For **4**, the IFD score was 5.41 kcal/mol in favor of the (2*S*,3*R*)-enantiomer. These *in silico* results are consistent with results disclosed in the patent literature, where (2*S*,3*R*)-**5** was described as the eutomer with respect to activation of α7 neuronal nicotinic receptors (*37*). The structural analysis (below) was therefore based on the models obtained for the (2*S*,3*R*)-enantiomers.

In order to validate the modeling procedure, the best scoring IFD solution obtained for nicotine was compared to 1UW6. It showed that the crystal conformations of both nicotine and the surrounding residues forming the binding site were reproduced with good accuracy: the rmsd for all atoms of the best scoring IFD pose was 1.27 Å and was 0.42 Å for the heavy atoms of nicotine only, compared with 1UW6. In addition, both experimentally determined hydrogen bonds anchoring nicotine in the active site (i.e., between the protonated amine and the main-chain carbonyl oxygen of Trp143 and between the pyridine nitrogen and the crystal water 1090) were correctly reproduced. The models were therefore concluded to be useful for describing the interactions of the different ligands with the AChBP-binding site.

The models illustrated that the main- and side-chain conformations of Val183−Tyr192 residues of the C loop, as well as side-chain conformations of residues surrounding the ligands, had adjusted in order to optimally accommodate each individual ligand. Whereas relatively minor conformational adjustments were observed for most residues lining the binding pocket, the effects of ligand binding on the conformation of loop C were more pronounced (the average rmsd for residues Val183−Tyr192 was 2.14 Å for all best scoring IFD complexes in comparison with 1UW6) and related to the size and shape of the ligands. Noteworthy in this respect is that nicotine, acetylcholine, epibatidine, and **1** in their best scoring IFD poses all had recruited

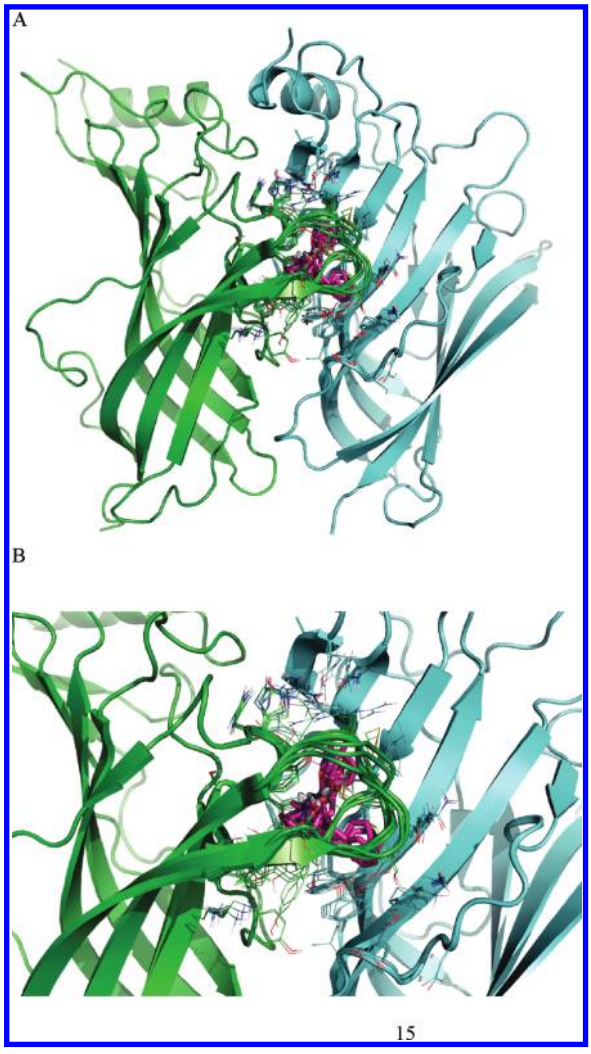

FIGURE 10: Molecular model of the Ls-AChBP ligand-binding site illustrating the flexibility of loop C and the residues surrounding acetylcholine, nicotine, epibatidine, and ligands **1**−**5**, superimposed in their best scoring IFD poses: (A) overview and (B) close-up. The binding site is located at the interface between two subunits, green and cyan. Ligands are rendered as magenta sticks. Amino acid residues within 5 Å of the ligands are rendered as lines.

the same starting loop conformation from the protein structure ensemble, although this was not the loop conformation that was most similar to the one in 1UW6.pdb.

The charged amino groups of all ligands in their best scoring IFD poses were located in the cation-binding pocket, surrounded by the aromatic side chains of Tyr89, Trp143, Tyr185, and Tyr192 of the A subunit and Trp53 and Tyr164 of the B subunit. This anchored the ligands in the binding site, and the orientation and interactions with other groups in the site were then defined by the other parts of the molecules. Acetylcholine formed a hydrogen bond between its ester carbonyl oxygen atom and a conserved water molecule (HOH1090 in 1UW6). This interaction was also mimicked by epibatidine and **1**, with their pyridine nitrogen atoms acting as H-bond acceptors. In addition, these two ligands also displayed an H-bond interaction between their protonated amines and the main-chain carbonyl of Trp143 of subunit A, in analogy with nicotine. Furthermore, the protonated amine of epibatidine formed an H-bond with the *p*-OH group of Tyr89 of subunit A (Figure 11).

The protonated quinuclidine of (2*S*,3*R*)-**2** interacted with the main-chain carbonyl of Trp143 of subunit A, similar to nicotine

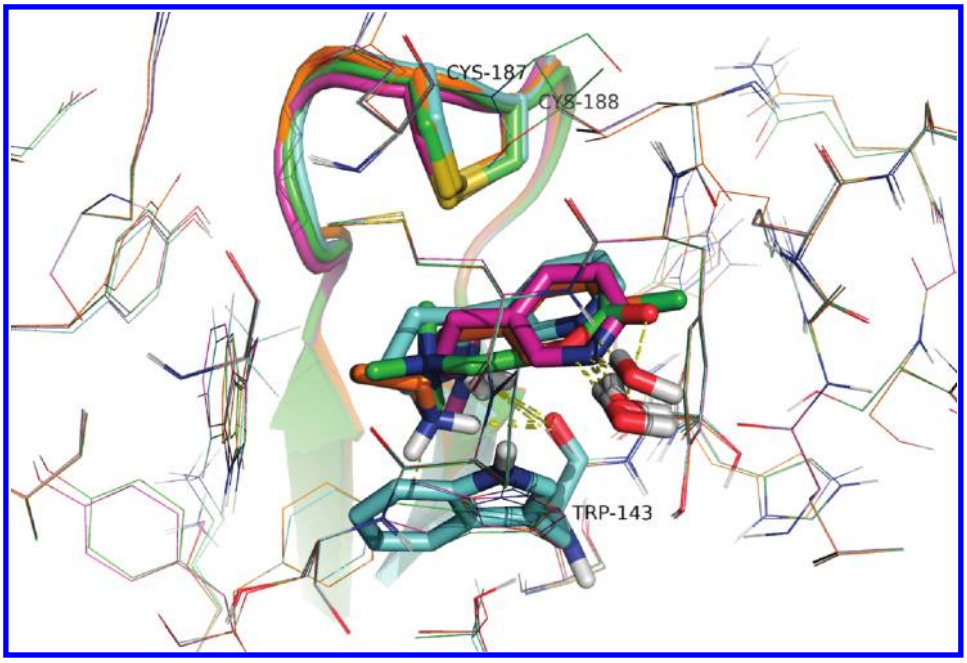

FIGURE 11: Superposition of the best scoring IFD poses of acetylcholine (green), nicotine (cyan), epibatidine (orange), and **1** (magenta), showing their common interactions with Trp143 and a conserved water. H-bonds are indicated as dashed yellow lines. C loops are rendered as cartoons in colors corresponding to the ligands.

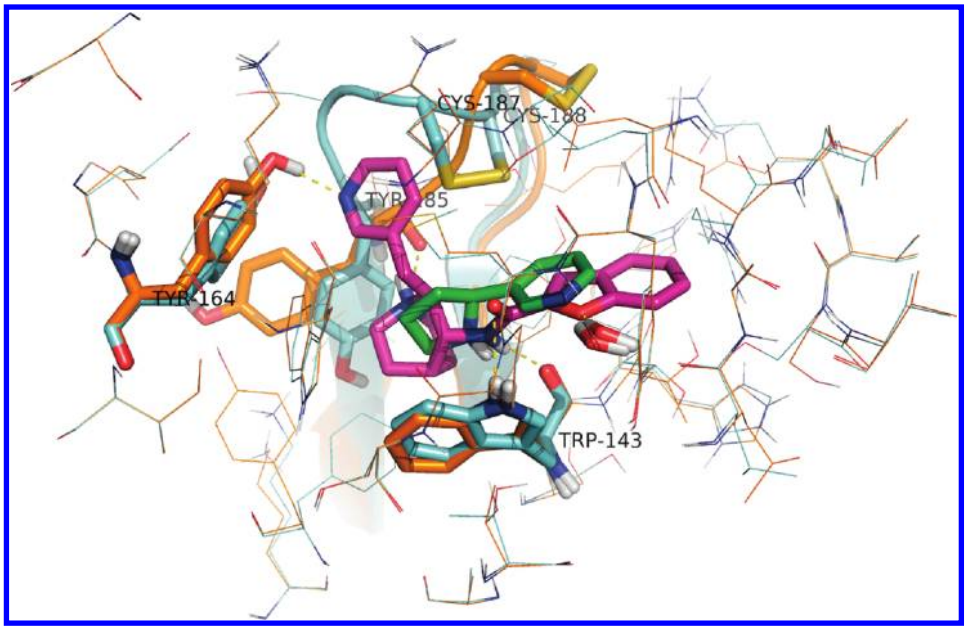

FIGURE 12: Superposition of the best scoring IFD pose of (2*S*,3*R*)-**5** (magenta) with the crystal conformation of nicotine (green). Protein structures corresponding to **5** and nicotine are colored orange and cyan, respectively. Residues forming H-bonds with **5** are rendered as sticks and C loops as cartoons. H-bonds are indicated as dashed yellow lines.

and epibatidine. Its pyridine group also occupied the same region as for nicotine, but did not mimic the H-bond with the conserved water. Instead, the pyridine nitrogen formed an H-bond with the side-chain hydroxyl group of Ser186 of loop C. For (2*S*,3*R*)-**3**−**5**, all bearing two large substituents on the quinuclidine ring system, the amide substituents occupied the pyridine pocket of nicotine, while their pyridinylmethyl groups were located near the N-terminal side of loop C, pointing toward Tyr164 in loop F of subunit B. The *p*-OH group of this residue formed an H-bond with the pyridine nitrogen atoms. Furthermore, the protonated quinuclidine nitrogen atoms formed H-bonds with the main-chain carbonyl group of Tyr185 of subunit A, while their amide NH groups mimicked the interaction of nicotine with the main-chain carbonyl group of Trp143 of subunit A. The side chains of Tyr185 and Tyr89 had rotated in order to optimally accommodate the quinuclidine cores, thus avoiding steric clashes with their aromatic rings. Furthermore, the conformation of loop C had adjusted considerably, in order to be able to accommodate the pyridinylmethyl groups, which otherwise would have clashed with Ser186 and Cys187. The binding mode of these compounds is exemplified by (2*S*,3*R*)-**5**, the most potent ligand of the series (Figure 12). For this particular ligand, an additional H-bond was present, involving the benzofuran oxygen atom and the conserved water that also interacts with the pyridine nitrogen atom of nicotine.

The molecular modeling thus shows that there are major differences in how the different ligands interact with AChBP.

This is evident in both their hydrogen-bonding patterns with a structural water, Tyr89, Trp143, Tyr164, Trp185, and Ser186 and the orientation of the side chains of Tyr89 and Tyr185. The importance of the tyrosine residues for the interactions prompted us to analyze their degree of conservation in the sequences of the human neuronal acetylcholine receptor α subtypes and Ls-AChBP. The analysis revealed a high level of conservation of the tyrosine residues observed to be involved in ligand interactions: Tyr89 and Tyr185 are present in all human α subtypes, except for α5. Tyr164 is present in α2, α3, and α7 and substituted for Phe in subtypes 1, 4, 6, 9, and 10. Tyr192 is present in all human α subtypes.

DISCUSSION

AChBP Biosensor Assay. A sensitive and informative biosensor-based assay for interaction studies of agonists with the Cys-loop receptor model protein AChBP was developed. The prepared surface had a comparatively high apparent binding capacity, allowing high-quality data to be obtained. The affinities for the three tested agonists agreed well with previously published values, i.e., acetylcholine, 458 vs 823 nM (*10*), nicotine, 40.7 vs 45.2 nM (*10*), and epibatidine, 0.0835 vs 0.16 nM (*22*), despite some differences in the buffer conditions. Interestingly, the corresponding values determined in the presence of DMSO were higher, indicating that this solvent had an effect on these interactions, either directly or indirectly via an effect on the structure. DMSO is a common additive to biochemical buffers, either as a cosolvent or as a consequence of DMSO stocks of the ligand molecules. It is a preferred solvent since it is miscible in water and has excellent solvating characteristics, a high boiling point, and a low toxicity. However, detrimental effects on biochemical and biophysical assays are common (*38*). The good solubility of acetylcholine, nicotine, and epibatidine allowed ligand interaction studies in the presence and absence of DMSO. The use of 5% DMSO in the buffer decreased both the affinity and the apparent binding capacity of the immobilized AChBP as compared to buffer without DMSO. The magnitude of these effects appeared to depend on the ligand, which might relate to the finding that conformational changes contribute to the observed signal amplitudes (see below). Both effects suggested that DMSO stabilized AChBP in a different conformation from the native one, similar to what has been reported for other proteins (*38*). This structural adaption to the buffer conditions must be kept in mind when comparing data from different experimental setups.

Nevertheless, it was concluded that a major part of the immobilized AChBP was functional with respect to its nicotine-binding site. This implicated the presence of intact oligomers on the sensor surface after immobilization. It is likely that a disruption of stacked pentamers would explain the large loss of preconcentrated material seen during deactivation of surfaces immobilized without cross-linking.

Kinetic Analysis of Agonist Binding. The interactions between the agonists and AChBP had affinities in the nanomolar range. However, the kinetics were very fast, and not all affinities could be dissected into rate constants due to mass transport limitations. Although interactions of small molecules with association rates over approximately 10^6 M^{-1} s^{-1} are influenced by limited mass transport, higher rate constants can still be determined when including a term for mass transport into the equation (*34*, *39*). Even if the determined rate constants might get increasingly unreliable with higher association rates, affinities are still valid from such data fittings (*34*, *40*). The clear dissociation signal observed for the AChBP ligands would normally allow for a determination of rate constants using SPR biosensor methodology, if the interaction was not influenced by limited mass transport. But, as demonstrated by the simulation, it is possible that the observed dissociation is an artifact resulting solely from a diffusion-controlled process.

Nevertheless, despite mass transport limitations, a few rate constants could be estimated. Regression analysis of sensorgrams for nicotine in buffer with DMSO from several experimental series returned congruent values for association and dissociation rate constants. The same interaction in buffer without DMSO was, however, completely governed by mass transport, and the regression analysis did not result in congruent values for k_{on} and k_{off}. It appears that DMSO mainly lowered the association rate for the nicotine interaction, even though from a visual comparison of the sensorgrams the dissociation seems to be mostly impaired (Figure 3). This also supported the conclusion that the interaction had much higher association rates in buffer without DMSO. The kinetics for acetylcholine were probably beyond what can be determined with the current instrumentation, irrespective of the conditions, and the actual rates are likely to be higher than indicated in Table 1.

A comparison of the values with those previously determined by tryptophan fluorescence quenching (*35*) showed that the dissociation rate constant was similar (3.62 vs 5.7 s^{-1}), whereas the association rate constant was 10 times lower (1.25×10^7 vs 1.5×10^8 M^{-1} s^{-1}). As for nicotine, the apparent association and dissociation rates for acetylcholine were also found to be much lower than determined previously by stopped flow (*41*). Since the buffer conditions for the stopped-flow measurements were not provided, it is not meaningful to speculate on the importance of any dissimilarities in the experimental conditions on the differences between the values and which values are the most reliable. It should also be remembered that SPR-based biosensors and stopped-flow instruments both have problems in quantifying very fast kinetic rate constants. For both techniques the limit of detection may be lower than the rates of agonist interactions with their receptors. It is therefore not possible to unequivocally establish how fast these interactions really are.

Although the rapid kinetics is problematic from an experimental point of view, they reveal important functional characteristics of neurotransmission. The binding and release of agonists have most likely evolutionarily been optimized to be very fast. The resulting "low" affinities as compared to interactions with slower dissociation rates are compensated for by the rapid and highly regulated change in agonist concentration. From a molecular recognition perspective it is interesting to note the structural features that have evolved for rapid interaction (see below).

Ligand-Induced Conformational Changes. The aim of the current investigation was to obtain an increased understanding of the mechanism of agonist interactions with Cys-loop receptors. It was therefore interesting to observe complexities in the SPR sensorgrams. Since deviations from simple interaction mechanisms are commonly a result of inappropriately performed or analyzed experiments, it was essential to exclude such artifacts and to see that they did not originate from simple mass absorption of the ligand to sensor surfaces. However, the observed complexities were interpreted as conformational changes and could be classified into two different processes with different kinetics, as schematically illustrated in Scheme 1. The scheme

represents a "minimalist model" that accounts for the interaction between agonist and receptor, the rapid conformational change corresponding to the opening and closing of the ion channel, and the slow conformational change involved in the desensitization of the receptor.

Conformational changes in immobilized proteins have previously been reported to result in SPR signals (*15*−*17*, *42*−*46*). A conformational transition might either be induced after a ligand has bound (i.e., induced fit; see, for example, ref *47*) or be required for the formation of the ligand-binding site and therefore occur before the ligand binds (i.e., selected fit; see, for example, ref *16*). Mixed forms are also possible, as illustrated by the combined induced and selected fit model (*48*). We have showed that for non-nucleoside inhibitor interactions with HIV-1 reverse transcriptase both selected fit and induced fit occur simultaneously and that minor changes in ligand or target structure determine the dominating pathway (*16*, *18*). Thus, the proposed model for AChBP can be seen as an extension of the combined induced and selected fit model, with an additional third dimension represented by the closed form (gray in Scheme 1). This system thus provides further evidence that conformational transitions of free and complexed proteins are important dynamic features involved in receptor and enzyme regulation.

Although AChBP does not contain the membrane spanning domain that constitutes the ion channel of mammalian Cys-loop receptors, the phenomena described here are likely to be relevant to conformational changes mediated by agonist in a receptor-coupled channel. This is supported by the remarkable experiments by Bouzat and colleagues, showing that when AChBP is linked to an ion channel and engineered for compatibility at the junction between binding and channel domains, agonist binding triggers opening and closing of the channel (i.e., a AChBP and 5HT3 chimera constitutes a functional ion channel) (*49*).

Slow Changes. Scheme 1 represents a model that accounts for the different steps known to be involved in Cys-loop receptor function. By simulation of sensorgrams based on this model, it can be concluded that the slow changes have observed rate constants in the 0.01 s^{-1} range and can correspond to the step described as desensitization. It can be excluded that the slow changes correspond to the structural adaption to ligand binding leading to the opening of the ion channel since they have been found to be very fast (*14*). Instead, desensitization has been described with similar slow kinetics for many receptors (for a review, see ref *50*). It can in the simplest case be described as a slow equilibrium change between receptor states, without necessarily changing the affinity between ligand and receptor dramatically. The isomerization between the resting state, the activated state, and the desensitized state is reversible, as originally described by Katz and Thesleff (*51*). This characteristic was confirmed in the experiments as the SPR signal always returned to the baseline of the resting state after interaction with a ligand. These equilibria are important for the development of ligands with therapeutic use, in the sense that it makes a difference if a compound stabilizes an ion channel in the open or in the desensitized state (*52*). The detection of slow conformational transitions associated with ligand binding might therefore constitute an important analytical tool for the design of new drugs.

Experimental evidence for this "structural footprint" that agonists leave on the receptor has been reported with a similar experimental setup using a biosensor with immobilized AChBP (*19*). These studies showed that agonist binding influences subsequent antagonist binding even after the agonist has dissociated. The results support the present findings and further address the structural nature and functional aspects of the agonist-induced slow conformational changes described here.

Fast Changes. A simple rule of thumb for SPR biosensor signal magnitudes is that the signal is proportional to the molecular weight of the analyte. After normalization for the molecular weight of the analyte, the maximum signal at steady state (R_{max}) is therefore expected to be the same for any analyte and can be used to determine the stoichiometry of an interaction and functionality of the immobilized protein. But it has previously been shown that SPR signals can also be "conformationally induced" by the binding of small molecules to a protein whose conformation changes upon the binding of the ligand (*15*−*17*, *44*, *46*).

In the present analysis of the interaction between AChBP and the studied ligands, there were significant differences in the maximal signal amplitudes for the different ligands. In contrast to the slow changes described above, these changes did not show up as complexities in the sensorgrams, i.e., deviations from a simple 1:1 interaction. This ligand-induced signal change can therefore be concluded to occur as fast, or faster, than the rates of the ligand binding. Moreover, the mechanism evidently involves ligand-specific structural rearrangements of AChBP since the normalized R_{max} values were correlated to the molecular volumes of the ligands.

Ligand-induced conformational changes in AChBP have been observed with other biophysical methods, including fluorescence spectroscopy (*22*, *41*, *53*, *54*), NMR (*54*), and hydrogen−deuterium exchange mass spectrometry (*55*). Structural changes have also been evident from analysis of crystal structures of AChBPs from various snail species with different ligands, mainly involving an adaptation of the position of loop C to the size of the ligand (*8*, *10*, *41*). Similar fluctuations in the receptor domain are assumed to trigger the opening and closing of the ion channel and are expected to result in quick equilibrium shifts between different conformer populations. Given that these processes result in SPR signal changes, these fast shifts would amplify or diminish the regular SPR signal from the mass adsorption process. New in the present report is the experimental evidence that the structural response correlates to the small differences in the ligand size.

A modeling procedure combining induced fit docking and selected loop flexibility was employed to generate individual binding hypotheses for the investigated ligands. This procedure has proven to generate reliable binding hypotheses for challenging systems, such as the induction of the DFG-out conformation by kinase inhibitors (*27*) and the blind prediction of a ligand-bound G-protein-coupled receptor structure (*56*). This, together with the fact that the binding mode of nicotine to Ls-AChBP could be reproduced with good accuracy, makes the obtained IFD poses for the other ligands also plausible. However, although this method aims at simulating the process of flexible receptor adaptation induced upon ligand binding, the final IFD poses merely comprise an ensemble of ranked solutions representing possible ligand-binding modes as present during steady-state kinetics. As such they cannot account for all of the time-resolved phenomena observed with SPR during exposure of Ls-AChBP to the ligands. Furthermore, only one flexible loop can currently be considered with this automated procedure, which is a limitation when more than one flexible loop is part of a ligand-binding site. For that reason, loop flexibility was restricted to loop C, known to be highly adaptable to ligands of different

nature. The gating mechanism of Cys-loop receptors, i.e., the propagation of structural rearrangements in the ligand-binding site to the pore domain upon ligand binding, can be studied in great detail using molecular dynamics simulations (see, e.g., ref *57*). However, such calculations are computationally demanding and hence unsuitable for comparing the conformational effects of series of compounds. Therefore, despite its shortcomings, the IFD protocol employed here was deemed a good trade-off between speed and accuracy for studying the problem at hand. The molecular modeling supported a mechanism where the signal involved a graded structural response depending on the size of the ligand. Significant ligand-dependent conformational changes were particularly obvious in loop C but were also seen in specific residues in the ligand-binding site. Notably, for the quinuclindine derivatives with the largest substituents (i.e., **3**−**5**), binding was associated with side-chain rotations of Tyr89 and Tyr185 (subunit A) and Tyr164 (subunit B). Interestingly, Tyr164 has previously been implicated in conformational changes of loop F induced by small-molecule agonists (*22*). The high degree of conservation of these tyrosine residues in human neuronal acetylcholine receptors suggests that they are also involved in ligand binding and signaling in humans.

Kinetics and Mechanisms of Neurotransmission. Under physiological conditions, local concentrations of acetylcholine fluctuate rapidly as a consequence of active release processes and inactivation by acetyl cholinesterase. Acetylcholine-mediated neurotransmission therefore requires rapid signaling mechanisms. Considering the permanent positive charge and small size of acetylcholine, as well as the lack of anionic residues in the ligand-binding site, the strong π−cation interactions are likely to be the driving force for the observed fast association rates of the ligands, acting at long distance. Once acetylcholine has bound to the cation pocket, the flexible loop C and residues surrounding the ligand-binding site instantaneously adopt the conformations needed to optimally embrace acetylcholine, resulting in downstream signal transduction. Although it is difficult at this stage to distinguish the structural changes corresponding to channel opening and desensitization, their different kinetics are indicative of their functions.

Conclusions. The present study provides further evidence that conformational changes in proteins can be detected with SPR-based biosensors. It has revealed mechanistic features of ligand interactions with AChBP that are expected to be significant for the understanding of Cys-loop receptor function. They confirm that the ligand−receptor interaction as such is very rapid and that it is possible to detect and distinguish rapid and slow conformational changes in the receptor upon binding of a ligand. The kinetics of the latter appears to correspond to the conformational changes responsible for receptor desensitization. It is expected that the newly developed interaction assay and the theoretical modeling will be useful tools for further exploration of the mechanism of Cys-loop receptor function and, ultimately, for identification of specific ligands suitable for pharmacological use toward this important class of ion channels.

REFERENCES

1. Sixma, T. K., and Smit, A. B. (2003) Acetylcholine binding protein (AChBP): a secreted glial protein that provides a high-resolution model for the extracellular domain of pentameric ligand-gated ion channels. *Annu. Rev. Biophys. Biomol. Struct. 32*, 311–334.
2. Smit, A. B., Celie, P. H., Kasheverov, I. E., Mordvintsev, D. Y., van Nierop, P., Bertrand, D., Tsetlin, V., and Sixma, T. K. (2006) Acetylcholine-binding proteins: functional and structural homologs of nicotinic acetylcholine receptors. *J. Mol. Neurosci. 30*, 9–10.
3. Cederholm, J. M., Schofield, P. R., and Lewis, T. M. (2009) Gating mechanisms in Cys-loop receptors. *Eur. Biophys. J. 39*, 37–49.
4. Ulens, C., Akdemir, A., Jongejan, A., van Elk, R., Bertrand, S., Perrakis, A., Leurs, R., Smit, A. B., Sixma, T. K., Bertrand, D., and de Esch, I. J. (2009) Use of acetylcholine binding protein in the search for novel alpha7 nicotinic receptor ligands. In silico docking, pharmacological screening, and X-ray analysis. *J. Med. Chem. 52*, 2372–2383.
5. Taly, A., Corringer, P. J., Guedin, D., Lestage, P., and Changeux, J. P. (2009) Nicotinic receptors: allosteric transitions and therapeutic targets in the nervous system. *Nat. Rev. Drug Discov. 8*, 733–750.
6. Smit, A. B., Syed, N. I., Schaap, D., van Minnen, J., Klumperman, J., Kits, K. S., Lodder, H., van der Schors, R. C., van Elk, R., Sorgedrager, B., Brejc, K., Sixma, T. K., and Geraerts, W. P. (2001) A glia-derived acetylcholine-binding protein that modulates synaptic transmission. *Nature 411*, 261–268.
7. Brejc, K., van Dijk, W. J., Smit, A. B., and Sixma, T. K. (2002) The 2.7 Å structure of AChBP, homologue of the ligand-binding domain of the nicotinic acetylcholine receptor, *Novartis Found. Symp.* 245, 22−29 (discussion 29−32, 165−168).
8. Bourne, Y., Talley, T. T., Hansen, S. B., Taylor, P., and Marchot, P. (2005) Crystal structure of a Cbtx-AChBP complex reveals essential interactions between snake alpha-neurotoxins and nicotinic receptors. *EMBO J. 24*, 1512–1522.
9. Brejc, K., van Dijk, W. J., Klaassen, R. V., Schuurmans, M., van Der Oost, J., Smit, A. B., and Sixma, T. K. (2001) Crystal structure of an ACh-binding protein reveals the ligand-binding domain of nicotinic receptors. *Nature 411*, 269–276.
10. Celie, P. H., van Rossum-Fikkert, S. E., van Dijk, W. J., Brejc, K., Smit, A. B., and Sixma, T. K. (2004) Nicotine and carbamylcholine binding to nicotinic acetylcholine receptors as studied in AChBP crystal structures. *Neuron 41*, 907–914.
11. Paas, Y., Gibor, G., Grailhe, R., Savatier-Duclert, N., Dufresne, V., Sunesen, M., de Carvalho, L. P., Changeux, J. P., and Attali, B. (2005) Pore conformations and gating mechanism of a Cys-loop receptor. *Proc. Natl. Acad. Sci. U.S.A. 102*, 15877–15882.
12. Monod, J., Wyman, J., and Changeux, J. P. (1965) On the nature of allosteric transitions: a plausible model. *J. Mol. Biol. 12*, 88–118.
13. Colquhoun, D., and Sakmann, B. (1981) Fluctuations in the microsecond time range of the current through single acetylcholine receptor ion channels. *Nature 294*, 464–466.
14. Sine, S. M., and Engel, A. G. (2006) Recent advances in Cys-loop receptor structure and function. *Nature 440*, 448–455.
15. Geitmann, M., and Danielson, U. H. (2004) Studies of substrate-induced conformational changes in human cytomegalovirus protease using optical biosensor technology. *Anal. Biochem. 332*, 203–214.
16. Geitmann, M., Unge, T., and Danielson, U. H. (2006) Biosensor-based kinetic characterization of the interaction between HIV-1 reverse transcriptase and non-nucleoside inhibitors. *J. Med. Chem. 49*, 2367–2374.
17. Christopeit, T., Gossas, T., and Danielson, U. H. (2009) Characterization of Ca^{2+} and phosphocholine interactions with C-reactive protein using a surface plasmon resonance biosensor. *Anal. Biochem. 391*, 39–44.
18. Elinder, M., Selhorst, P., Vanham, G., Öberg, B., Vrang, L., and Danielson, U. (2010) Inhibition of HIV-1 by non-nucleoside reverse transcriptase inhibitors via an induced fit mechanism—Importance of slow dissociation and relaxation rates for antiviral efficacy, *Biochem. Pharmacol.* (in press).
19. Retra, K., Geitmann, M., Kool, J., Smit, A. B., De Esch, I. J., Danielson, U. H., and Irth, H. (2010) Development of SPR biosensor assays for primary and secondary screening of AChBP ligands, *Anal. Biochem.* (in press).
20. Kasheverov, I. E., Zhmak, M. N., Fish, A., Rucktooa, P., Khruschov, A. Y., Osipov, A. V., Ziganshin, R. H., D'Hoedt, D., Bertrand, D., Sixma, T. K., Smit, A. B., and Tsetlin, V. I. (2009) Interaction of alpha-conotoxin ImII and its analogs with nicotinic receptors and acetylcholine-binding proteins: additional binding sites on *Torpedo* receptor. *J. Neurochem. 111*, 934–944.
21. Paulo, J. A., and Hawrot, E. (2009) A radioisotope label-free alpha-bungarotoxin-binding assay using BIAcore sensor chip technology for real-time analysis. *Anal. Biochem. 389*, 86–88.
22. Hibbs, R. E., Radic, Z., Taylor, P., and Johnson, D. A. (2006) Influence of agonists and antagonists on the segmental motion of residues near the agonist binding pocket of the acetylcholine-binding protein. *J. Biol. Chem. 281*, 39708–39718.
23. Sherman, W., Day, T., Jacobson, M. P., Friesner, R. A., and Farid, R. (2006) Novel procedure for modeling ligand/receptor induced fit effects. *J. Med. Chem. 49*, 534–553.
24. Mazurov, A., Klucik, J., Miao, L., Phillips, T. Y., Seamans, A., Schmitt, J. D., Hauser, T. A., Johnson, R. T., Jr., and Miller, C. (2005)

2-(Arylmethyl)-3-substituted quinuclidines as selective alpha 7 nicotinic receptor ligands. *Bioorg. Med. Chem. Lett. 15*, 2073–2077.
25. Markgren, P. O., Lindgren, M. T., Gertow, K., Karlsson, R., Hämäläinen, M., and Danielson, U. H. (2001) Determination of interaction kinetic constants for HIV-1 protease inhibitors using optical biosensor technology. *Anal. Biochem. 291*, 207–218.
26. Karlsson, R., Katsamba, P. S., Nordin, H., Pol, E., and Myszka, D. G. (2006) Analyzing a kinetic titration series using affinity biosensors. *Anal. Biochem. 349*, 136–147.
27. Sherman, W., Beard, H. S., and Farid, R. (2006) Use of an induced fit receptor structure in virtual screening. *Chem. Biol. Drug Des. 67*, 83–84.
28. Zhu, K., Pincus, D. L., Zhao, S., and Friesner, R. A. (2006) Long loop prediction using the protein local optimization program. *Proteins 65*, 438–452.
29. Friesner, R. A., Banks, J. L., Murphy, R. B., Halgren, T. A., Klicic, J. J., Mainz, D. T., Repasky, M. P., Knoll, E. H., Shelley, M., Perry, J. K., Shaw, D. E., Francis, P., and Shenkin, P. S. (2004) Glide: a new approach for rapid, accurate docking and scoring. 1. Method and assessment of docking accuracy. *J. Med. Chem. 47*, 1739–1749.
30. Halgren, T. A., Murphy, R. B., Friesner, R. A., Beard, H. S., Frye, L. L., Pollard, W. T., and Banks, J. L. (2004) Glide: a new approach for rapid, accurate docking and scoring. 2. Enrichment factors in database screening. *J. Med. Chem. 47*, 1750–1759.
31. Friesner, R. A., Murphy, R. B., Repasky, M. P., Frye, L. L., Greenwood, J. R., Halgren, T. A., Sanschagrin, P. C., and Mainz, D. T. (2006) Extra precision glide: docking and scoring incorporating a model of hydrophobic enclosure for protein-ligand complexes. *J. Med. Chem. 49*, 6177–6196.
32. Duffy, E. M., and Jorgensen, W. L. (2000) Prediction of properties from simulations: free energies of solvation in hexadecane, octanol, and water. *J. Am. Chem. Soc. 122*, 2878–2888.
33. DeLano, W. (2002) The PyMOL Molecular Graphics System, DeLano Scientific, Palo Alto, CA.
34. Karlsson, R. (1999) Affinity analysis of non-steady-state data obtained under mass transport limited conditions using BIAcore technology. *J. Mol. Recognit. 12*, 285–292.
35. Hansen, S. B., Radic, Z., Talley, T. T., Molles, B. E., Deerinck, T., Tsigelny, I., and Taylor, P. (2002) Tryptophan fluorescence reveals conformational changes in the acetylcholine binding protein. *J. Biol. Chem. 277*, 41299–41302.
36. Babakhani, A., Talley, T. T., Taylor, P., and McCammon, J. A. (2009) A virtual screening study of the acetylcholine binding protein using a relaxed-complex approach. *Comput. Biol. Chem. 33*, 160–170.
37. Bencherif, M., Benson, L., Dull, G. M., Fedorov, N. B., Gatto, G. J., Genus, J., Jordan, K. G., Mathew, J., Mazurov, A. A., Miao, L., Munoz, J. A., Pfeiffer, I., Pfeiffer, S., and Phillips, T. Y. (2008) (2S,3R)-N-(2-((3-pyridinyl)methyl)-1-azabicyclo[2.2.2]oct-3-yl-benzyofuran-2-carboxamide, novel salt forms, and methods of use thereof (WO2009/018505, Ed.).
38. Somasundaran, P. (2004) Encyclopedia of Surface and Colloid Science, Vol. 7, 2nd ed., Taylor & Francis, London.
39. Myszka, D. G., He, X., Dembo, M., Morton, T. A., and Goldstein, B. (1998) Extending the range of rate constants available from BIACORE: interpreting mass transport-influenced binding data. *Biophys. J. 75*, 583–594.
40. Önell, A., and Andersson, K. (2005) Kinetic determinations of molecular interactions using Biacore—Minimum data requirements for efficient experimental design. *J. Mol. Recognit. 18*, 307–317.
41. Hansen, S. B., Sulzenbacher, G., Huxford, T., Marchot, P., Taylor, P., and Bourne, Y. (2005) Structures of Aplysia AChBP complexes with nicotinic agonists and antagonists reveal distinctive binding interfaces and conformations. *EMBO J. 24*, 3635–3646.
42. Sota, H., Hasegawa, Y., and Iwakura, M. (1998) Detection of conformational changes in an immobilized protein using surface plasmon resonance. *Anal. Chem. 70*, 2019–2024.
43. Mannen, T., Yamaguchi, S., Honda, J., Sugimoto, S., Kitayama, A., and Nagamune, T. (2001) Observation of charge state and conformational change in immobilized protein using surface plasmon resonance sensor. *Anal. Biochem. 293*, 185–193.
44. Gestwicki, J. E., Hsieh, H. V., and Pitner, J. B. (2001) Using receptor conformational change to detect low molecular weight analytes by surface plasmon resonance. *Anal. Chem. 73*, 5732–5737.
45. May, L. M., and Russell, D. A. (2002) The characterization of biomolecular secondary structures by surface plasmon resonance. *Analyst 127*, 1589–1595.
46. Flatmark, T., Stokka, A. J., and Berge, S. V. (2001) Use of surface plasmon resonance for real-time measurements of the global conformational transition in human phenylalanine hydroxylase in response to substrate binding and catalytic activation. *Anal. Biochem. 294*, 95–101.
47. Geitmann, M., and Danielson, U. H. (2004) Studies of substrate-induced conformational changes in human cytomegalovirus protease using optical biosensor technology. *Anal. Biochem. 332*, 203–214.
48. Weikl, T. R., and von Deuster, C. (2009) Selected-fit versus induced-fit protein binding: kinetic differences and mutational analysis. *Proteins 75*, 104–110.
49. Bouzat, C., Gumilar, F., Spitzmaul, G., Wang, H. L., Rayes, D., Hansen, S. B., Taylor, P., and Sine, S. M. (2004) Coupling of agonist binding to channel gating in an ACh-binding protein linked to an ion channel. *Nature 430*, 896–900.
50. Quick, M. W., and Lester, R. A. (2002) Desensitization of neuronal nicotinic receptors. *J. Neurobiol. 53*, 457–478.
51. Katz, B., and Thesleff, S. (1957) A study of the desensitization produced by acetylcholine at the motor end-plate. *J. Physiol. 138*, 63–80.
52. Buccafusco, J. J., Beach, J. W., and Terry, A. V., Jr. (2009) Desensitization of nicotinic acetylcholine receptors as a strategy for drug development. *J. Pharmacol. Exp. Ther. 328*, 364–370.
53. Gao, F., Bren, N., Burghardt, T. P., Hansen, S., Henchman, R. H., Taylor, P., McCammon, J. A., and Sine, S. M. (2005) Agonist-mediated conformational changes in acetylcholine-binding protein revealed by simulation and intrinsic tryptophan fluorescence. *J. Biol. Chem. 280*, 8443–8451.
54. Gao, F., Mer, G., Tonelli, M., Hansen, S. B., Burghardt, T. P., Taylor, P., and Sine, S. M. (2006) Solution NMR of acetylcholine binding protein reveals agonist-mediated conformational change of the C-loop. *Mol. Pharmacol. 70*, 1230–1235.
55. Shi, J., Koeppe, J. R., Komives, E. A., and Taylor, P. (2006) Ligand-induced conformational changes in the acetylcholine-binding protein analyzed by hydrogen-deuterium exchange mass spectrometry. *J. Biol. Chem. 281*, 12170–12177.
56. Michino, M., Abola, E., Brooks, C. L., III, Dixon, J. S., Moult, J., and Stevens, R. C. (2009) Community-wide assessment of GPCR structure modelling and ligand docking: GPCR Dock 2008. *Nat. Rev. Drug Discov. 8*, 455–463.
57. Cheng, X., Wang, H., Grant, B., Sine, S. M., and McCammon, J. A. (2006) Targeted molecular dynamics study of C-loop closure and channel gating in nicotinic receptors. *PLoS Comput. Biol. 2*, e134.